The Fatigue and Fracture Resistance of a Nb-Cr-Ti-Al Alloy

D.L. DAVIDSON and K.S. CHAN

The microstructure, fatigue, and fracture behaviors of a cast and heat-treated Nb-Cr-Ti-Al alloy were investigated. The microstructure of the cast alloy was manipulated by annealing at a temperature ranging from 500 °C to 1500 °C for 1 to 24 hours. The heat treatment produced Cr_2Nb precipitates along grain boundaries in all cases except in the 500 °C heat-treated material. Fracture toughness tests indicated low fracture resistance in both the as-cast and heat-treated materials. Fatigue crack growth tests performed on the 500 °C heat-treated material also indicated a low fatigue crack growth resistance. Direct observations of the near-tip region revealed a cleavage-dominated fracture process, in accordance with fractographic evidence. The fracture behavior of the Nb-Cr-Ti-Al alloy was compared to that of other Nb-Cr-Ti alloys. In addition, theoretical calculations of both the unstable stacking energy (USE) and Peierls–Nabarro (P–N) barrier energy are used to elucidate the role of Al additions in cleavage fracture of the Nb-Cr-Ti-Al alloy. The results indicate that an Al alloying addition increases the USE, which, in turn, prevents the emission of dislocations, promotes the nucleation and propagation of cleavage cracks from the crack tip, and leads to a reduction in the fracture toughness.

I. INTRODUCTION

RECENT studies have shown that fracture toughness on the order of 10 to 20 MPa$\sqrt{m}$ can be achieved in Nb-based *in situ* composites, based on the Nb-Cr-Ti,[1,2,3] Nb-Si,[4–7] Nb-Al-Ti,[8,9] and Nb-Ti-Hf-Cr-Al-Si[10–13] systems. These materials are characterized by a two-phase microstructure comprised of intermetallic and metallic solid-solution phases. For composites of engineering interest, the intermetallic phase exists in the form of hard particles embedded in a solid-solution metallic matrix. In the Nb-Cr-Ti system, the intermetallic particles are Cr_2Nb, which is a Laves phase with the C15 structure at ambient temperature.[14,15] The Cr_2Nb particles are brittle, with a fracture toughness of about 1 MPa$\sqrt{m}$.[1,2,3] Because of the low toughness of the particles, most, if not all, of the fracture toughness of the *in situ* composites, based on the Nb-Cr-Ti system, originates from the matrix, which is a Nb solid-solution containing Cr and Ti.

It has been demonstrated that a Ti addition in the range from 30 to 40 at. pct enhances the fracture resistance of Nb-Cr alloys by reducing the Peirels–Nabarro (P–N) barrier energy and stress, thereby increasing the dislocation mobility.[16] This has the effect of promoting the emission of dislocations and suppressing the propagation of cleavage cracks from the crack tip. As a result, the plane-strain fracture toughness of Nb-Cr-Ti solid-solution alloys increases with increasing Ti contents. The presence of hard Cr_2Nb particles increases the plastic constraint in the matrix and reduces the fracture resistance if the matrix phase does not have sufficient ductility. With a ductile Nb solid-solution matrix, a fracture toughness as high as 20 MPa$\sqrt{m}$ has been achieved in Nb/Cr_2Nb *in situ* composites containing 38 vol pct Cr_2Nb particles.

The oxidation resistance of Nb-Cr-Ti solid-solution alloys and *in situ* composites, however, is inadequate for high-temperature applications. One possible means of increasing the oxidation resistance is to add Al to Nb-Cr-Ti to form solid-solution alloys and *in situ* composites based on the Nb-Cr-Ti-Al system. An example of the former is Nb-40Ti-10Cr-10Al and, of the latter, is Nb-27Ti-10Cr-24A1.[10] Other alloying strategies include the addition of Hf and Si, which have been used to produce a variety of *in situ* composites based on a solid-solution matrix with either silicide particles, $(Nb,Ti,Cr)_2Al$, or $(Nb,Ti,Hf)_2Al$ particles.[10] The characteristics of these emerging alloys and *in situ* composites have been summarized in recent review articles.[9–13]

The effect of an Al addition on the fatigue and fracture properties of Nb-Cr-Ti-Al alloys is not well understood. Limited previous work on Nb-40Ti-10Cr-10Al indicated that the addition of Al to Nb-Cr-Ti solid-solution alloys led to a reduction in the fracture toughness.[3,16] When correlated to the fracture toughness of other Nb-Cr-Ti alloys on the basis of the number of d + s electrons per atom in the system, the Nb-40Ti-10Cr-10Al alloy showed a negative deviation from the trend line of increasing toughness with decreasing number of d + s electrons per atom.[2] Previous work also indicated that an Al addition can cause a reduction in the tensile ductility of Nb-Cr-Ti-Al alloys.[9] The mechanism responsible for the decrease in the fracture toughness and tensile ductilty with an Al addition has not been established.

The objective of this article is to report findings on the microstructure, fatigue, and fracture behavior of a cast Nb-Ti-Cr-Al alloy. The results of this alloy are compared to those of cast Nb-Ti-Cr and Nb-Ti-Cr-Al alloys in the literature to determine the effect of an Al alloying addition on the fatigue and fracture resistance and the controlling fracture mechanism. In order to elucidate this effect, theoretical calculations of the unstable stacking energy (USE) and (P–N) barrier energy are performed to estimate the ease of dislocation nucleation at the crack tip and the dislocation mobility.

D.L. DAVIDSON and K.S. CHAN, Institute Scientists, are with the Southwest Research Institute, San Antonio, TX 78238.

Manuscript submitted November 3, 1998.

Table I. A summary of LANL-Made Nb-Cr-Ti-Al Alloys Investigated in This Study

Alloy Designation	Composition (At. Pct)				Interstitials (Ppm, Wt)	
	Nb	Cr	Ti	Al	O	N
LANL-2	37*	36*	27*	—	690	18
LANL-3	47.2	11.2	32.3	8.3	820	60

*Target composition; actual values were not measured.

II. EXPERIMENTAL PROCEDURES

A. *Materials*

Three ingots were prepared at Los Alamos National Laboratory (LANL, Los Alamos, NM) from pure elements using the plasma arc melting method.[17] The three elements were melted in a 10-cm-diameter water-cooled copper hearth. Each alloy was remelted six times to ensure homogeneous distribution of the elements. Two sound ingots were obtained, while the third one was not tested because of chemical inhomogeneity. One of the sound materials was similar to compositions from which previous results had been obtained, and the other included aluminum because of its effect of increasing the oxidation resistance of Nb alloys. Each ingot weighed approximately 1.8 kg. The designations of the two sound alloys and the actual compositions are shown in Table I. Also in the table are the levels of interstitials measured by LANL.

B. *Screening Tests*

The ingots were screened for microstructures and mechanical properties, to ensure that they exhibited the desired characteristics, before detailed fatigue and fracture tests were performed. Optical microscopy, energy-dispersive spectroscopy, hardness tests, and fracture testing on small bend bars were used for the screening tests.

The microstructure of alloy 37Nb-36Cr-27Ti (herein termed LANL-2) contained continuous networks of Cr_2Nb particles along grain boundaries. This microstructure had previously been found to produce a low fracture toughness because of cracking along the grain boundaries.[2] Consequently, only a small effort was expended to screen the mechanical properties of this material. Fracture toughness values of 7.6 and 6.8 MPa$\sqrt{m}$ were measured using notched three-point-bend specimens.

The ingot of alloy 47.2Nb-11.2Cr-32.3Ti-8.3Al (herein termed LANL-3) was cut axially in half using electro-discharge machining (EDM), and a second cut was made to produce a slice approximately 3-mm thick. One side of this slab was polished and was found to have several regions which exhibited different light-diffraction and contrast conditions. A region of high porosity was found in the center in the last part of the ingot solidified. The hardness was measured at several locations on the slice and was found to be somewhat different.

The slice taken from the ingot of LANL-3 was cut by EDM into four compact-tension (CT) specimens approximately 25 mm squared and into two beams suitable for three-point-bend fracture-toughness specimens. The composition of two of the CT specimens was checked by energy-dispersive X-ray microprobe and found to be within less than 1 at. pct of the desired composition. The fracture toughness of the as-received alloy was measured, using a three-point-bend specimen, as 18.5 MPa$\sqrt{m}$. Optical microscopy revealed only a single-phase microstructure. The LANL-3 alloy was selected for studies to investigate fatigue and fracture resistance as a function of microstructure.

C. *Microstructures*

One of the possible reasons for the low fracture toughness of the as-received material was that the matrix contained a high dislocation content, resulting from phase transformations and thermal stresses induced by differences in the coefficients of thermal expansion between the constituent phases. Thus, heat treatment might recover, or possibly recrystallize, the matrix, thereby reducing flow resistance and increasing fracture toughness. Based on this reasoning, a series of heat treatments was conducted. The as-received material was encapsulated and given a 1-hour anneal at a selected temperature followed by a furnace cool. The annealing temperatures were 1000 °C, 1200 °C, 1350 °C, or 1500 °C. Heat treatments at 500 °C for 6 hours and at 900 °C for 24 hours were also attempted, to recover the matrix.

The X-ray diffraction technique was used to determine the lattice parameter of the matrix and of the Cr_2Nb, as well as the volume fraction of Cr_2Nb. The X-ray diffraction was conducted at 40 kV and 30 mA, using a Cu target. All the peaks found during X-ray diffraction were either from the matrix or Cr_2Nb, except for the heat treatment at 1350 °C, which resulted in 13 peaks that are unidentified. The volume fraction of intermetallic was estimated from the intensity of the {311} peak from Cr_2Nb, with the {110} peak of the matrix normalized to an intensity of 100 pct.

The grain size was measured from the as-cast material and from one of the specimens that was heat treated to 500 °C for 6 hours. The grain size was determined from the number of intercepts of grain boundaries along a straight line. The grain size measured in this way was 230 $\pm$ 60 μm.

D. *Fatigue and Fracture Testing*

To gage the effects of heat treatment on mechanical properties, Vickers hardness tests, fatigue crack growth, and fracture toughness were measured. The CT specimens were used for both the fatigue and fracture tests. All but one specimen was notched and fatigue precracked under cyclic tensile loads, at a ratio (R) of 0.1, a starting ΔK value of 5 MPa$\sqrt{m}$, and a frequency of 10 Hz. One of the fracture-toughness specimens was tested in the notched condition without a fatigue precrack. Fatigue and fracture-toughness tests were performed in a servohydraulic testing machine and in a scanning electron microscope (SEM) equipped with a loading stage.[18] Fatigue tests were performed in air outside the SEM, and specimens were periodically placed in the SEM for *in situ* observations of the fatigue crack growth process and characterization of the near-tip deformation behavior. Fracture toughness tests were conducted in the SEM exclusively. To characterize the fracture process, the near-tip region was photographed as a function of the stress intensity factor and crack extension. Still photographs of the near-tip region, under the unloaded and loaded conditions, were analyzed *via* a machine vision–based stereoimaging technique[19] to obtain the near-tip displacement and strain fields. Fractography was performed on both the fatigue and fracture surfaces using scanning electron microscopy.

III. RESULTS

A. *Microstructure*

The as-received LANL-3 material, shown in Figure 1(a), showed a single-phase, large-grained microstructure with an average grain size of 230 μm. With the exception of the 500 °C heat-treatment, the heat-treated materials all showed a two-phase microstructure containing precipitates mostly on the grain boundaries. Many of the grain-boundary precipitates were continuous, but some took a pearl string–like morphology, as illustrated in Figures 1(c) through (f). Both are expected to lead to poor fracture toughness. The second-phase particles were unexpected, because the Nb-Cr-Ti ternary-phase diagram suggested a single-phase solid solution. Apparently, the addition of Al altered the phase boundary, leading to the formation of the second-phase particles on grain boundaries. The 500 °C heat treatment showed no Cr_2Nb precipitation in most areas when examined by optical microscopy, but one area, Figure 1(b), appeared to show some particles. Transmission electron microscopy was not performed on this material. Thus, submicron-sized particles not resolved by optical microscopy could exist in this microstructure.

Table II lists the heat treatments, measured values of hardness, fracture toughness, and volume fraction of Cr_2Nb. The hardness value is the average of at least ten measurements, while the fracture-toughness value and the volume fraction of Cr_2Nb are for an individual specimen. It was apparent from these results that heating caused the hardness to change from the as-received value, with a minimum at 500 °C for 6 hours, as shown in Figure 2. The increased hardness probably meant that Cr_2Nb was being precipitated. Examination of the material using X-ray diffraction indicated no intermetallic in the as-received material and showed that heat treatment led to the precipitation of Cr_2Nb. The hardness trend is inconsistent with the amount of Cr_2Nb that was caused by heat treatment, as determined by X-ray diffraction. Using X-ray peak intensity to estimate the volume fraction is known to have limited accuracy; perhaps this is the reason for the inconsistency.

Table II. The Effects of Heat Treatment on Hardness, Fracture Toughness, and Volume Fraction of Cr_2Nb Particle of the LANL-3 Alloy

Number	Heat Treatment: Temperature, °C	Heat Treatment: Time, h	Vickers Hardness (kg/mm^2)	Fracture Toughness (MPa$\sqrt{m}$)	Volume Fraction of Cr_2Nb (Pct)
1	as received	—	435	12.6, 15.5, 18.5	0
2	500	6	372	11.7, 15.2	0
3	1000	1	392	12.8	7.6
4	1200	1	410	—	3.7
5	1350	1	425	—	11
6	1500	1	432	—	1.2
7	900	24	485	—	8.1

B. *Lattice Parameters*

Lattice parameters of the matrix and of Cr_2Nb are listed in Table III. The relationship between the amount of intermetallic and the lattice parameter is shown in Figure 3. The structure of C15 is cubic, and its unit cell is close to twice the size of the unit cell of the bcc matrix; thus, half the lattice parameter of Cr_2Nb is shown in the figure. The difference between the two can be considered to be the strain between the two lattices that would be required for them to be coherent. The average strain determined (Table III) is about 7.5 pct, and there is no consistent variation with heat treatment or amount of intermetallic.

The lattice parameter of Cr_2Nb decreases with the addition of Ti, according to Thoma,[15] as follows:

$$\begin{aligned}&\text{Half the lattice parameter of } Cr_2Nb\\&= 3.5125 - 0.00015 \text{ (at. pct Ti)}\end{aligned} \qquad [1]$$

If the data in Figure 3 are combined with Eq. [1], then it implies that the Cr_2Nb that has precipitated in the alloy due to heat treatment incorporates Ti, because the lattice parameter decreases with volume of Cr_2Nb precipitated. When this occurs, the lattice parameter of the matrix increases because Ti has been removed by the formation of Cr_2Nb(Ti). Diffusion of Ti from the matrix to Cr_2Nb lowers the incoherency strains between the two phases, as seen in Table III.

The presence of Cr_2Nb in this alloy, with only 11 at. pct Cr, appears to indicate that the amount of Cr that could be kept in solid solution was lowered by the addition of Al from about 15 at. pct to maybe half that amount, or less. Since the hardness was lowered somewhat by heat treatment at 500 °C, it was concluded that this treatment recovered the matrix with the precipitation of a minimum of intermetallic and would make the matrix more deformable.

C. *Fatigue Crack Growth*

Measurements of fatigue crack growth made from two CT specimens of LANL-3 are shown in Figure 4. These specimens were cycled at $R = 0.1$ in air at 10 Hz. Both specimens were heat treated to 500 °C for 6 hours in vacuum. The first specimen (CT-1) broke unexpectedly while cycling in the laboratory machine at $K_c = 11.7$ MPa$\sqrt{m}$. The crack in the second specimen (CT-2) was grown under $5 < \Delta K < 14$ MPa$\sqrt{m}$. Several times, this specimen was transferred to the SEM loading stage for measurement of crack-opening load and to make photographs of the crack-tip region for subsequent analysis. This specimen broke while being loaded in the SEM stage, giving a fracture toughness of $K_c = 15.2$ MPa$\sqrt{m}$. Crack-opening loads were directly measured in the SEM at $K = 6.9$, 7.2, and 14 MPa$\sqrt{m}$. As a fraction of the maximum load, the opening loads for these ΔK levels were 0.65, 0.79, and 0.76, respectively.

Fatigue crack growth in this heat treatment of LANL-3 may be typified as being "intermittently critical" because of occasional and sudden, rapid crack growth. During one experiment, while the specimen was being loaded in the SEM, the crack grew nearly 50 μm and then arrested. This characteristic of crack growth is illustrated in Figure 5, where the lack of a smooth curve indicates the erratic nature of crack growth. The large scatter shown in Figure 4 is also thought to result from this crack growth behavior.

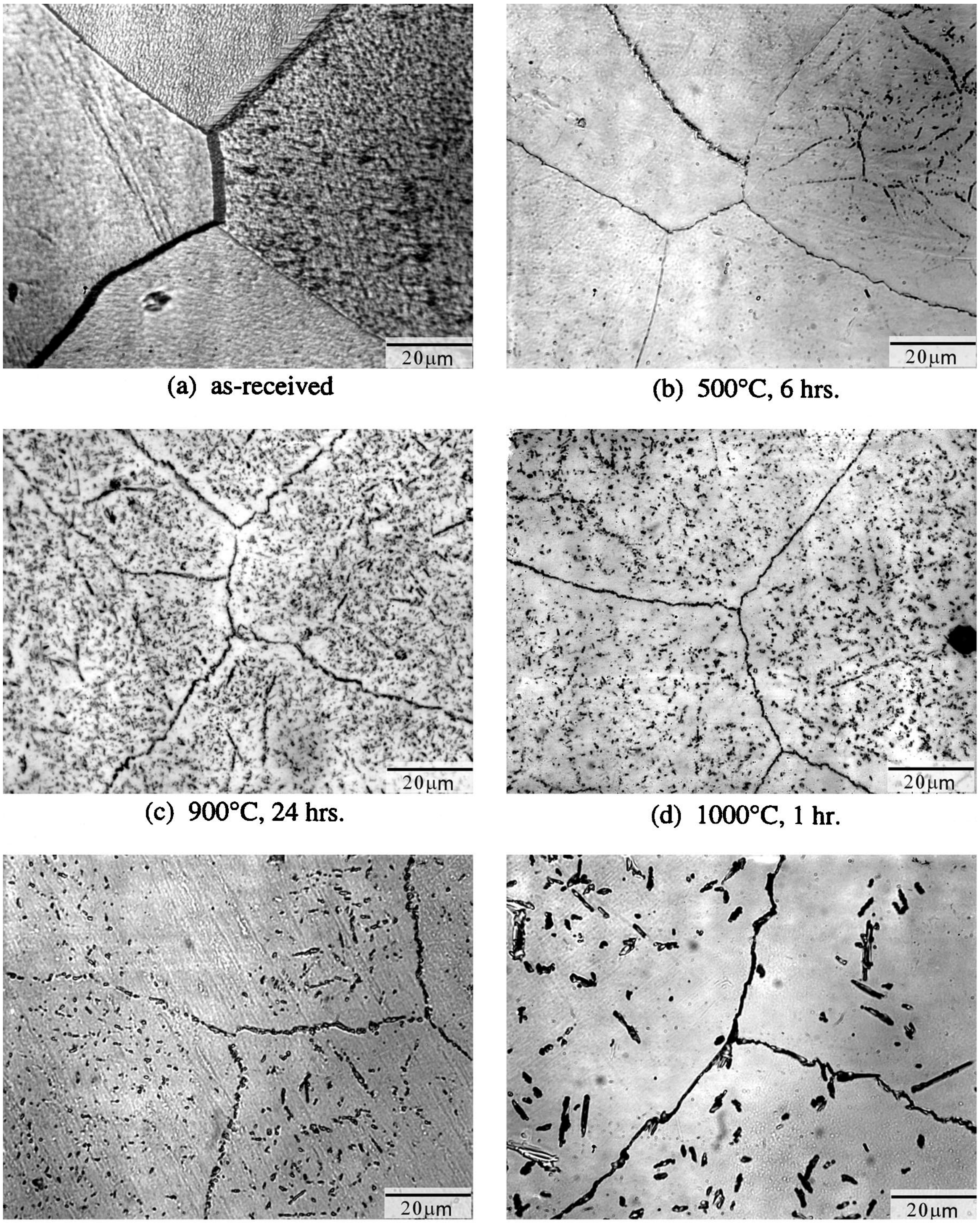

Fig. 1—Microstructures of LANL-3 (46Nb-11Cr-34Ti-9Al) in various heat-treatment conditions: (*a*) as-cast; (*b*) 500 °C, 6 h, (*c*) 900 °C, 24 h; (*d*) 1000 °C, 1 h; (*e*) 1200 °C, 1 h; and (*f*) 1500 °C, 1 h.

1. *Crack-tip analyses*

Figures 6 through 8 show micromechanical analyses of the crack region at two interesting locations. The analysis shown in Figure 6 is for a crack growing approximately parallel to a grain boundary. Apparently, the grain on the right-hand side is more-favorably oriented for slip; thus, the plasticity within that grain is greater than in the grain containing the crack. The crack tip seen in Figure 7 is at the same location, but the analysis is at higher resolution, showing that within the grain containing the crack tip, the strain distribution is relatively smooth, with two shear bands emanating from the tip at high angles to the direction of crack growth, which is typical for a blunted crack tip. The grain boundary does not appear to cause a disturbance in the strain distribution.

The crack tip in the analysis shown in Figure 8 is within

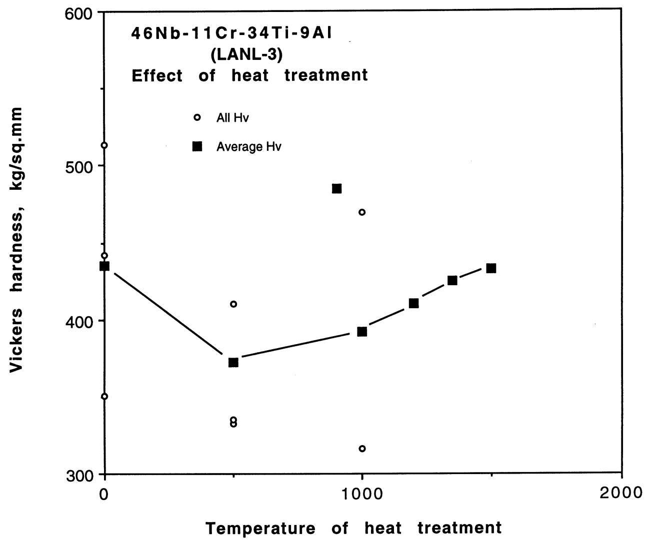

Fig. 2—Hardness *vs* heat-treatment temperature for the 46Nb-11Cr-34Ti-9Al alloy, designated as LANL-3. Each data point represents the average of ten hardness readings.

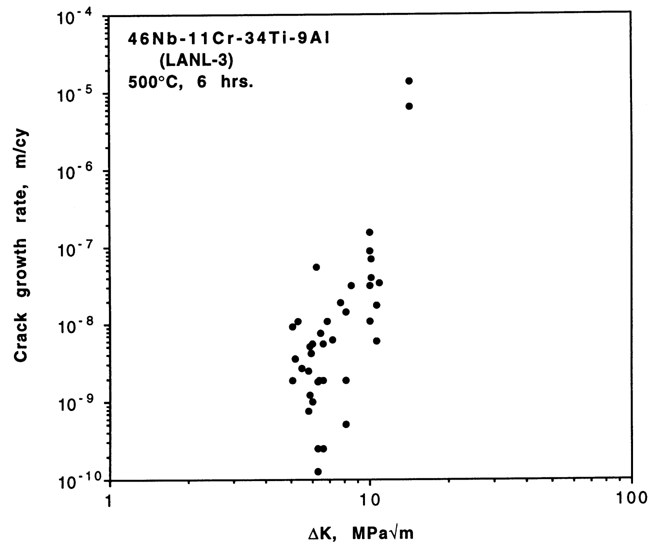

Fig. 4—Fatigue crack growth rate for LANL-3 heat treated to 500 °C for 6 h.

Table III. Lattice Parameters and Strain of the LANL-3 Alloy

Heat Treatment	Lattice Parameter Matrix (A)	Lattice Parameter Cr_2Nb (A)	Cr_2Nb (Vol Pct)	Lattice Strain (Pct)
As received	3.2380	—	0	—
500 °C/6 h	3.2388	—	0	—
1000 °C/1 h	3.2453	7.0253	7.5	8.2
1200 °C/1 h	3.2712	7.0007	3.7	7.0
1350 °C/1 h	3.2646	6.9791	11	6.9*
1500 °C/1 h	3.2406	7.0007	1.2	8.0
900 °C/24 h	3.3170	7.1385	8.1	7.6

*Thirteen extra diffraction peaks.

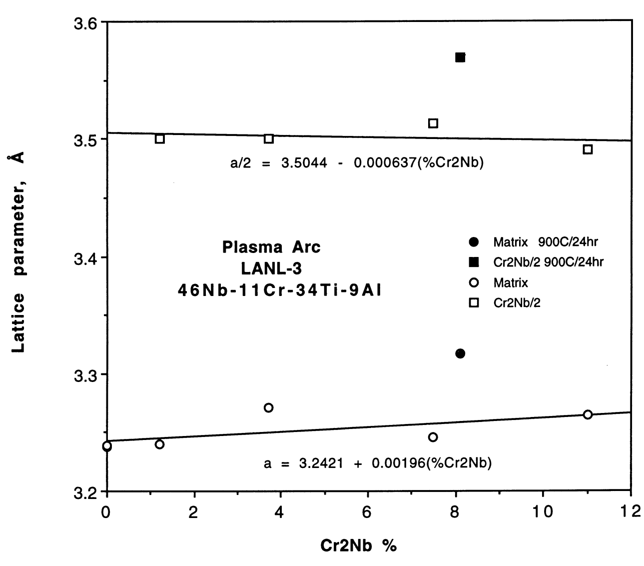

Fig. 3—Correlation between measured lattice parameters of matrix and intermetallic with amount of intermetallic, as determined by X-ray diffraction.

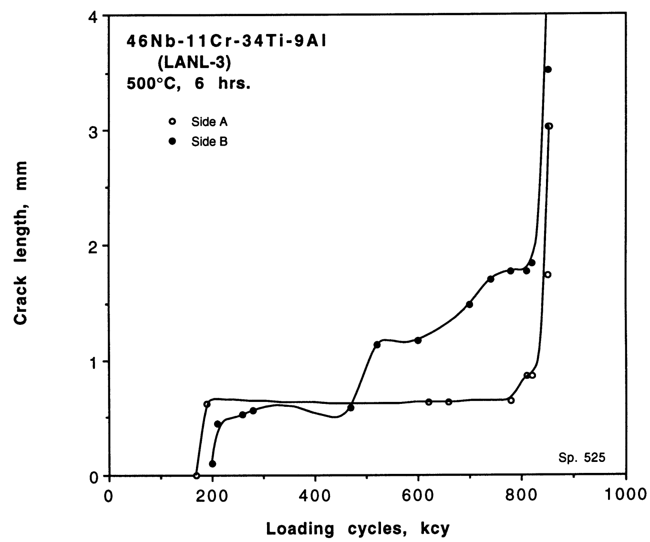

Fig. 5—An example of the highly erratic nature of crack growth.

2 μm of a grain boundary that is about 80 deg to the direction of the crack growth. Stereoimaging indicated that what appears to be a crack parallel to the grain boundary was not opening due to the applied load. However, the misorientation of slip systems between the two grains has affected the distribution of strain much more than shown in the other samples.

2. *Fractography*

The fracture surface of LANL-2, shown in Figure 9, exhibited an extremely brittle appearance. The cleavage facets could appear to be mainly transgranular, but some intergranular failure may also be seen. Much of the debris seen on the fracture surface is probably Cr_2Nb particles dislodged from the grain boundaries during fracture.

The fracture surfaces of LANL-3 are shown in Figures 10 and 11. Fatigue striations (periodic crack-arrest marks) are seen on many transgranular fracture planes in Figure 10(a). The higher-magnification view of Figure 10(b) shows

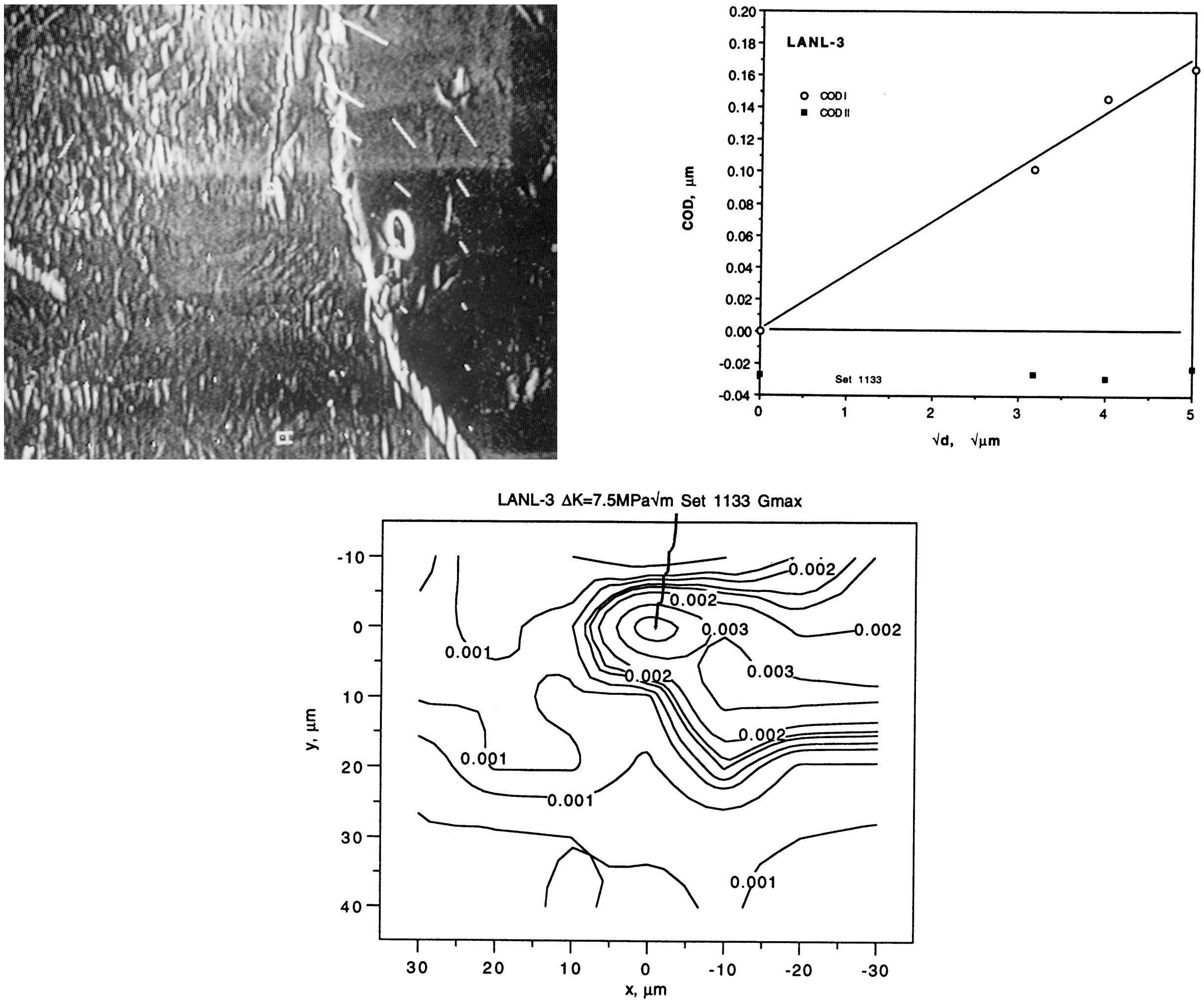

Fig. 6—Fatigue crack growth through LANL-3 at ΔK = 7.5 MPa$\sqrt{m}$, approximately parallel to a grain boundary and 12 μm from it. Microanalysis indicated that the grain on the right was deforming easier than the grain containing the crack tip.

the striations better and indicated that the average spacing (about 2.5 μm) of the striations is much larger than the average crack growth rate (about 0.2 μm/cycle).

The fractography of fast fracture is shown in Figure 11. Planar surfaces at many angles to the loading axis, some nearly parallel to it, may be seen in Figure 11(a), and many of these fracture facets have little topography. The detail in Figure 11(b) shows that there are indications of slip on planes at an angle to the fracture plane; thus, the material flowed plastically during failure.

D. *Fracture Toughness*

The fracture-toughness values for several microstructures of the LANL-3 material are listed in Table II. The K resistance (K_R) curves for the as-received material are shown in Figure 12 for notched specimens with and without a fatigue precrack. The two K_R curves show that the onset of crack extension occurred at low K values (5 to 11 MPa$\sqrt{m}$) with moderate slopes, indicating that the material is brittle and that plastic flow at the notch root is limited. For the cracked specimen, the onset of crack extension occurred at 11 MPa$\sqrt{m}$. The fracture resistance increased to 14 MPa$\sqrt{m}$ with a crack extension of $\approx$1300 μm. At 14.8 MPa$\sqrt{m}$, the crack propagated and caused ultimate fracture at $\approx$15.5 MPa$\sqrt{m}$. For the notched specimen, crack initiation occurred at a K level that is less than 8 MPa$\sqrt{m}$, and the fracture resistance increased with crack extension to $\approx$12.6 MPa$\sqrt{m}$ at the onset of ultimate fracture.

A summary of the fracture process in the notched specimen is presented in Figure 13, which shows the near-tip region of the main crack at K = 8 MPa$\sqrt{m}$. Examination of the crack tip at high magnification revealed that there was little plastic flow in the near-tip region and that there was no emission of slip from the crack tip. The crack path in Figure 13 showed a series of cleavage cracks and grain-boundary cracks separated by intact, though small, ligaments. Most of these ligaments were located between cleavage cracks and were able to sustain some plastic deformation, as shown in Figure 14. In other cases, the ligaments were located between cleavage cracks and grain-boundary cracks. The presence of these ligaments in the crack wake gave rise to the resistance-curve behavior observed in this alloy. Eventually, these small ligaments were fractured upon loading, and the specimen failed at K = 12.6 MPa$\sqrt{m}$.

Figure 15 shows the near-tip region of the fatigue-precracked specimen at K = 11 MPa$\sqrt{m}$. A cleavage microcrack formed ahead of the main crack during fatigue. This

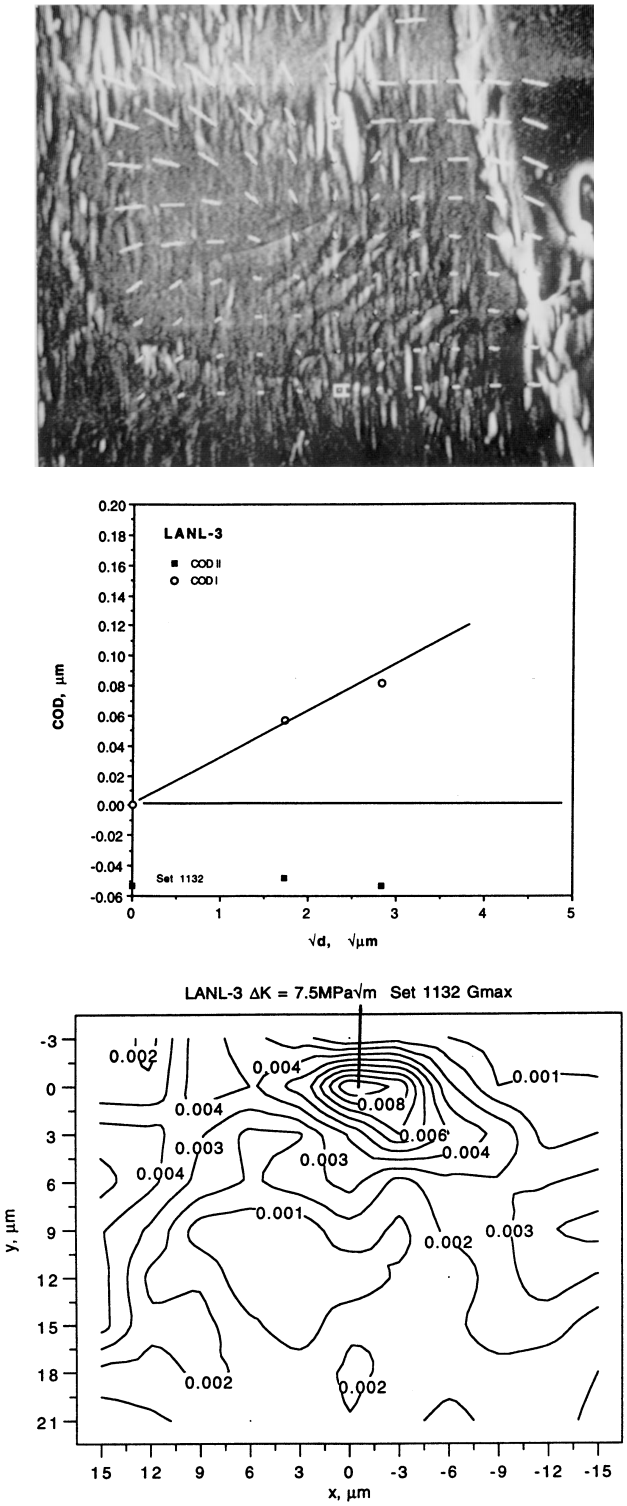

Fig. 7—A more detailed analysis of the crack tip shown in Fig. 6. A shear band emanates from the crack tip on the right side.

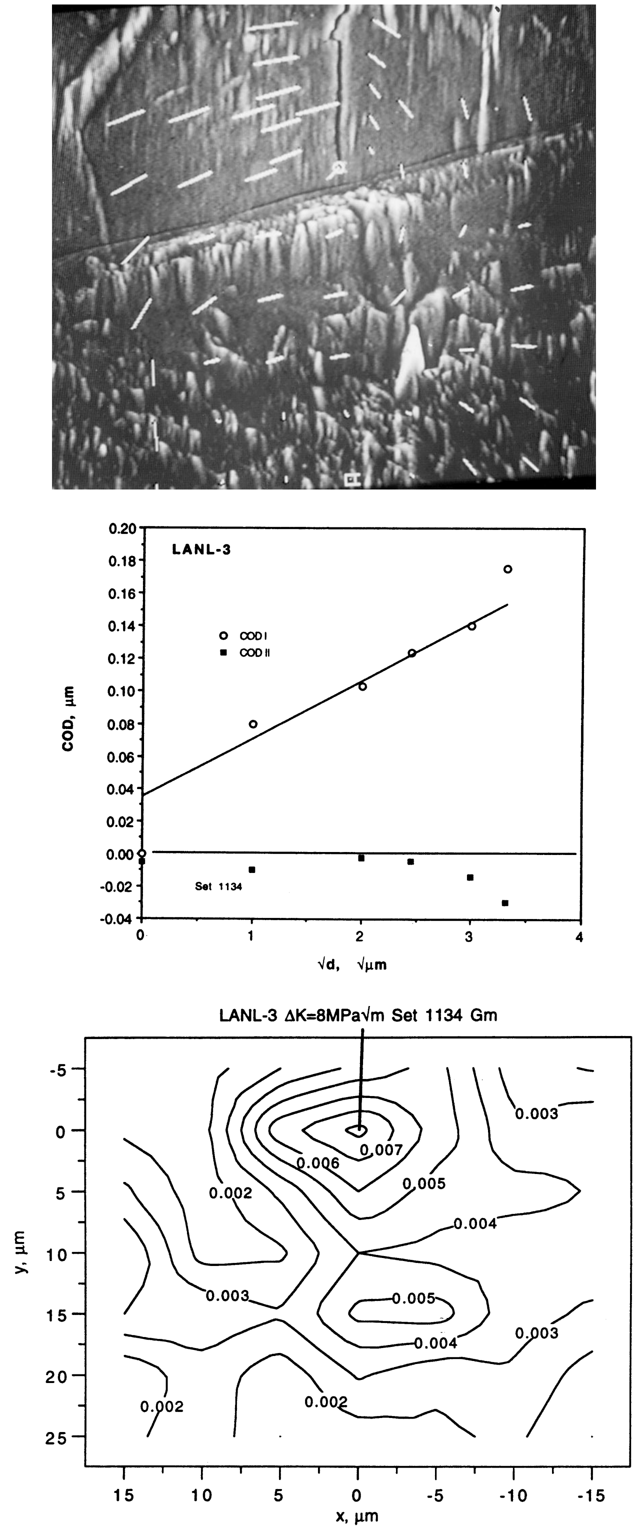

Fig. 8—Fatigue crack growth through LANL-3 at $\Delta K = 8.0$ MPa$\sqrt{\text{m}}$. The crack tip is approximately 2 μm from a grain boundary, and the crack is growing nearly perpendicular to it. There appears to be a crack parallel to the grain boundary; however, it did not open when the specimen was loaded. Microanalysis indicated that the strain distribution was disrupted by the differences in slip characteristics between the two grains.

cleavage microcrack opened up when the main crack was loaded. At 11 MPa$\sqrt{\text{m}}$, the crack grew toward the microcrack, reducing the width of the interconnecting ligament, while the tips of the microcracks deflected and extended to lie normal to the applied stress. When K was increased to 14 MPa$\sqrt{\text{m}}$, at least two cleavage cracks nucleated and propagated unstably over a distance of $\approx$1300 μm, running through grains and along grain boundaries (Figure 15(b)). The cracks eventually all arrested. The crack path contained a few small ligaments which remained intact at $K = 14.8$

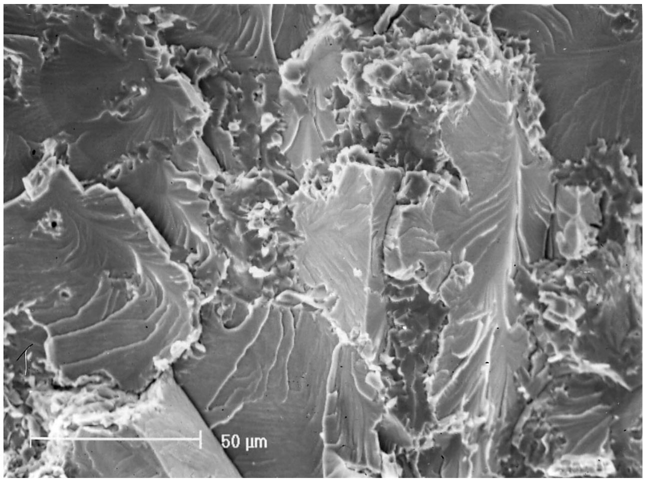

Fig. 9—Fractography for LANL-2 showing the generally brittle nature of the fracture process. The crack path appears to be a combination of transgranular and intergranular fracture. Some of the very fine features seen are interpreted as being failure through the intermetallic within grain boundaries.

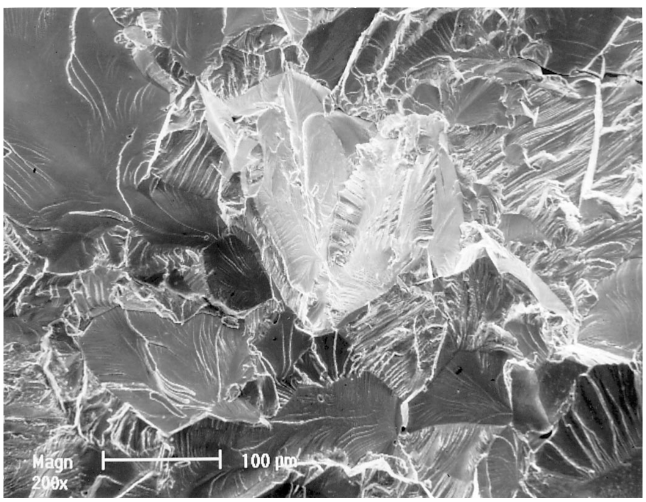

(*a*)

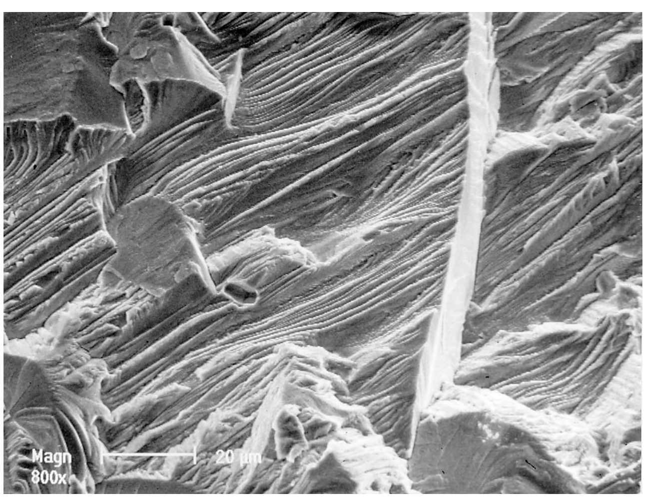

(*b*)

Fig. 10—(*a*) and (*b*) Fractography of fatigue crack growth in LANL-3 at about $\Delta K = 8$ MPa$\sqrt{\text{m}}$. Crack growth was from bottom to top. The periodic markings are interpreted as being crack arrest marks (fatigue striations).

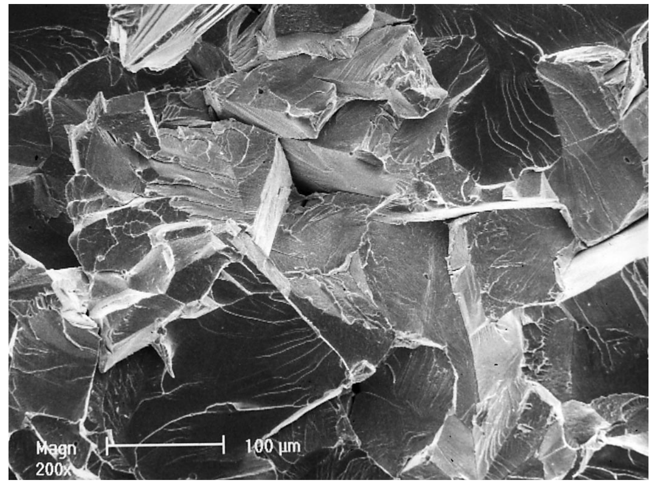

(*a*)

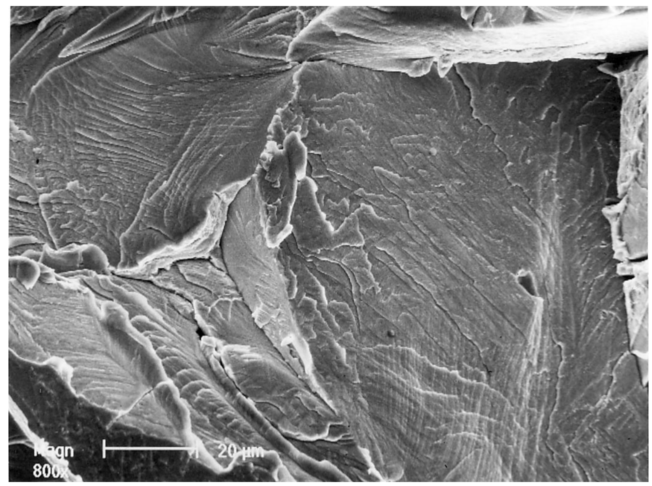

(*b*)

Fig. 11—(*a*) and (*b*) Fractography of fast fracture in LANL-3. Crack growth was from bottom to top. Crack growth was very planar, but on many different planes, some nearly parallel to the loading axis. The detail in (b) shows what are interpreted as slip lines intersecting the fracture surface on the right side and curved edges in other areas. These features are indicative of plasticity.

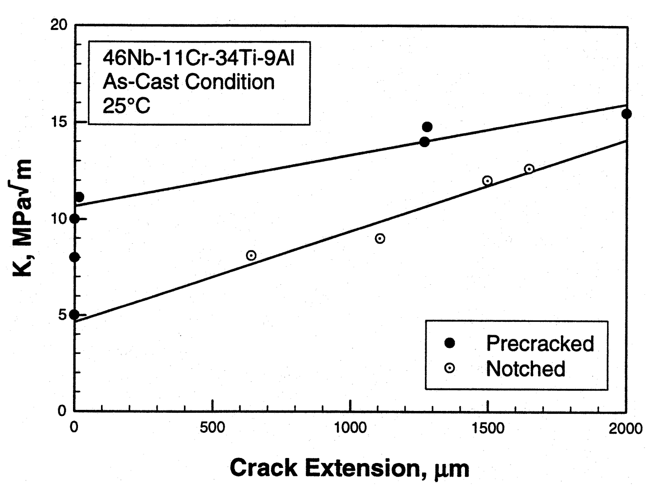

Fig. 12—*K*-resistance curves of 46Nb-11Cr-34Ti-9Al.

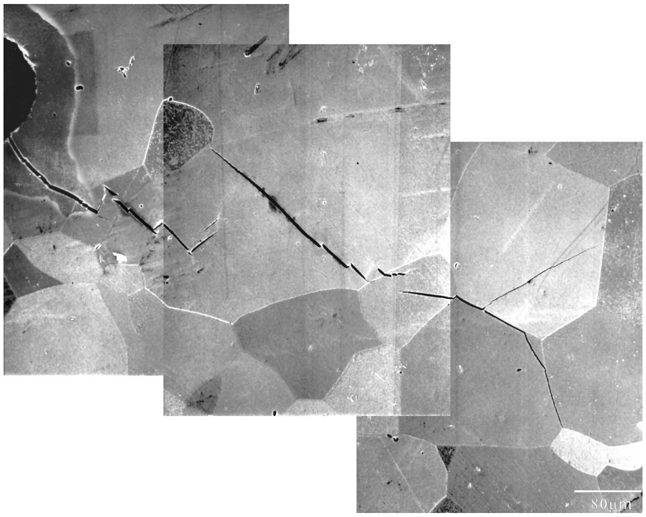

Fig. 13—A summary of the fracture process in 46Nb-11Cr-34Ti-9Al. The crack path shows a series of arrested cleavage and grain boundary cracks separated by intact ligaments.

MPa$\sqrt{m}$, but the specimen fractured at K = 15.5 MPa$\sqrt{m}$ when these ligaments failed.

1. *Crack-tip analysis*

The near-tip displacement and strain fields of the main crack just before the nucleation of cleavage cracks (K = 11 MPa$\sqrt{m}$) are shown in Figures 15(a) and (c), respectively. From Figure 15(a), it appears that emission of slip or dislocations from the crack tip did not happen. Instead, two cleavage cracks formed in the process zone and propagated across the entire grain (Figure 15(b)). The locations of the two cleavage cracks, shown as the dashed lines in Figure 15(c), were strained only lightly and elastically; cleavage cracks occurred with little plastic deformation. There was, however, some plastic deformation within the ligament in the crack wake, which led to the resistance-curve fracture behavior manifested by the alloy.

2. *Fractography*

The fracture surfaces of the as-received alloy exhibited mostly cleavage facets, as shown in Figure 16(a). Many of the facets showed the river-line pattern characteristic of cleavage I. Some of the facets corresponded to grain-boundary fracture facets, and they showed some evidence of slip within the grain and slip impingement at the grain boundary (Figure 16(b)). The extent of plastic flow, however, appeared to be quite limited, since the lengths of slip lines were very short.

IV. DISCUSSION

The composition of alloy LANL-3 is a variation of one of the alloys previously studied[16] which showed very high fracture toughness ($>$60 MPa$\sqrt{m}$). The difference between these two alloys is that, in LANL-3, a substitution of some Al was made for Cr. This addition of Al resulted in the precipitation of Cr_2Nb on grain boundaries during heat treatment, while the previous alloy contained no intermetallic. Because of cracking of grain-boundary particles, the heat-treated materials showed lower fracture toughness values than the as-cast material, which does not have Cr_2Nb particles. In the 500 °C heat treatment, precipitated intermetallic particles were not detected by X-ray diffraction or metallographically at 2000 times magnification. However, the particles could have been too small to image (less than about 15 μm) and of too low a volume fraction to be detected by X-rays. This heat treatment resulted in a decrease in hardness, which has been interpreted as recovery of the matrix and an indication of the absence of precipitation of intermetallic.

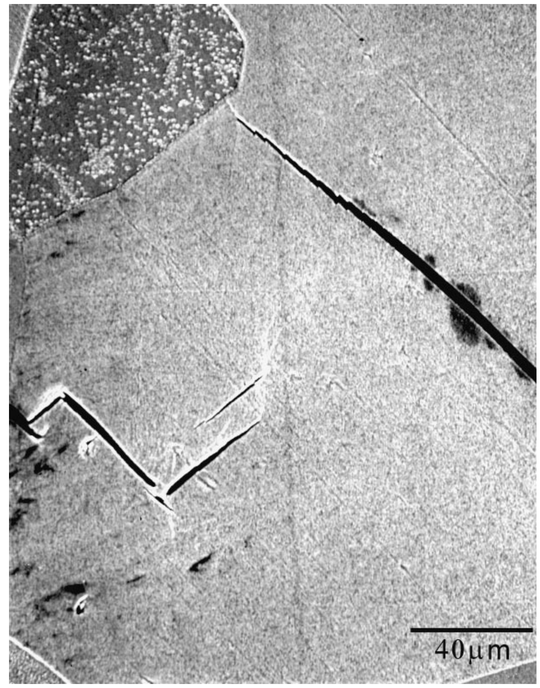

(*a*)

(*b*)

Fig. 14—(*a*) and (*b*) Plastic deformation in a ligament located between two parallel cleavage cracks. The crack-wake ligaments are responsible for the resistance-curve fracture behavior.

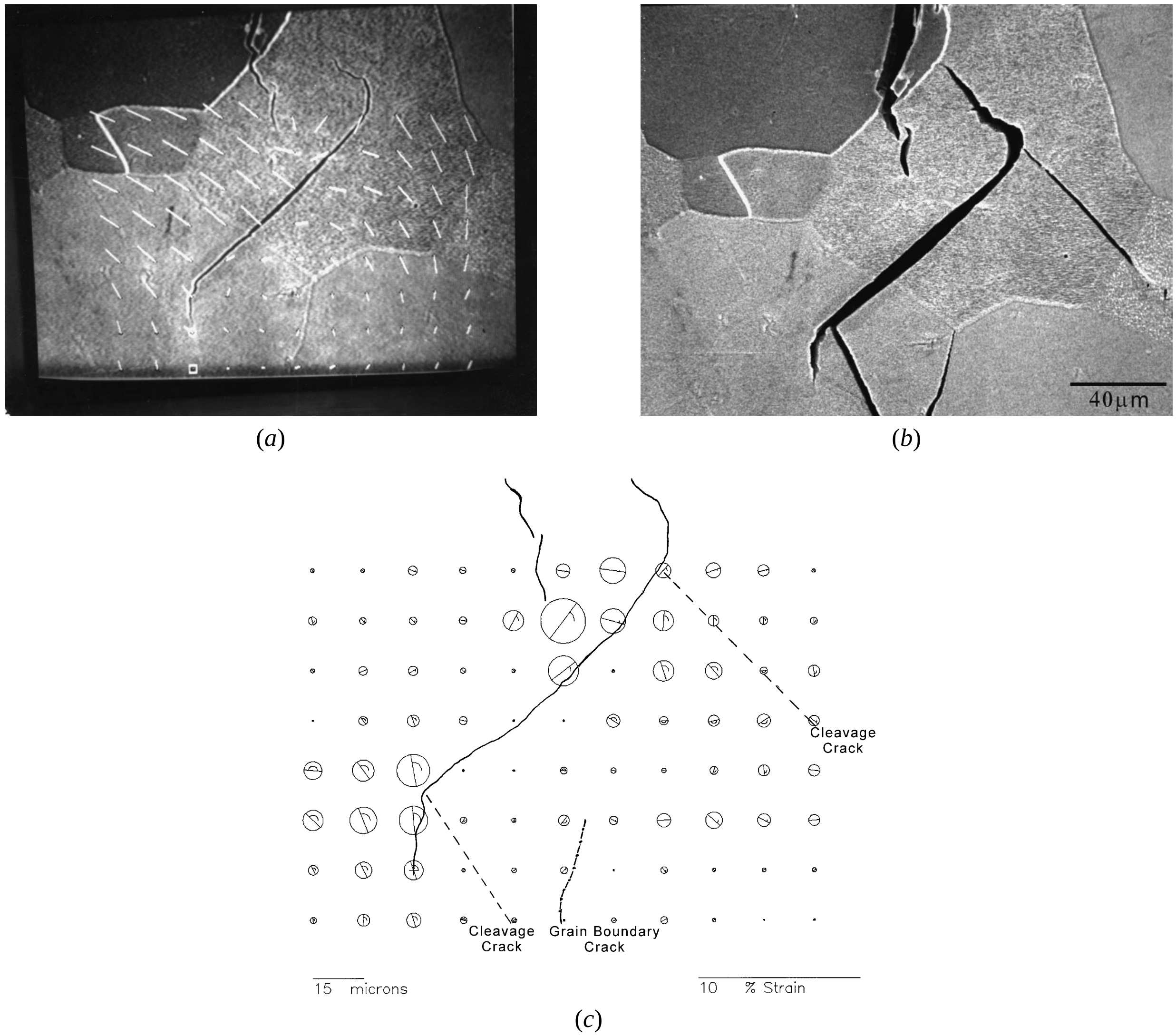

Fig. 15—Crack-tip displacement and strain fields of the main crack in 46Nb-11Cr-34Ti-9Al at $K = 11$ MPa$\sqrt{\text{m}}$ before the nucleation of cleavage cracks: (*a*) displacement field at $K = 11$ MPa$\sqrt{\text{m}}$ superimposed on a micrograph of the near-tip region, (*b*) near-tip region at $K = 14$ MPa$\sqrt{\text{m}}$, and (*c*) strain field at $K = 11$ MPa$\sqrt{\text{m}}$ superimposed with cleavage cracks (dashed lines) and a grain boundary crack (dot-dashed line). Crack growth was from top to bottom.

The fracture toughness of the 500 °C heat-treated material is essentially identical to that of the as-received alloy.

A comparison of the fracture-resistance curves of the Nb-Cr-Ti-Al and Nb-Cr-Ti solid-solution alloys is presented in Figure 17, which indicates that the Nb-Cr-Ti-Al alloy is less fracture resistant than the Nb-Cr-Ti alloy. In particular, the plane-strain initiation toughness of the Nb-Cr-Ti alloy is reduced from 34 to 14 MPa$\sqrt{\text{m}}$ with a 9 at. pct Al addition. The present result is consistent with the fracture toughness of 23 MPa$\sqrt{\text{m}}$ reported for Nb-40Ti-10Cr-10Al.[3,16]

Figure 18 shows a comparison of the fatigue crack growth curve of the Nb-Cr-Ti-Al alloy to that of the tough Nb-Cr-Ti alloy reported earlier.[25] It is evident that the former is considerably less fatigue resistant than the latter alloy, by virtue of a steeper slope. As alluded to earlier, the steep slope in the *da*/*dN* curve for the Nb-Cr-Ti-Al alloy was the consequence of an intermittently critical crack extension process, where cleavage cracks nucleated and propagated over a substantial distance.

Recent work[26] indicated that as little as 4 at. pct Al led to an ordered B2 structure in Ti-V-Cr alloys. The possibility exists that an Al addition in Nb-Cr-Ti can result in ordering in the matrix and lead to a reduction in fracture resistance. Ordered B2 alloys have been developed and studied extensively by researchers at Ohio State University.[8,27] Ordering has also been reported in Nb-Cr-Ti-Al alloys.[9] Some of the ordered B2 alloys, however, exhibited high ductility and fracture toughness at ambient temperature.[8,27] Thus, it is uncertain whether or not ordering is responsible for the lowering of fracture toughness in Nb-Cr-Ti alloy by Al additions.

Instead, it is thought that an aluminum addition to Nb-Cr-Ti affected the interatomic bonding, such that cleavage fracture is favored over dislocation emission from the crack tip. A measure of the propensity for dislocation nucleation from a crack tip is the USE,[20] while a measure of the mobility of dislocations moving away from the crack tip is the P–N barrier energy or stress.[21,22] Estimates of the USE and P–N barrier energy were made using the equations of Rice[20] and Wang,[23,24] respectively, *via* the

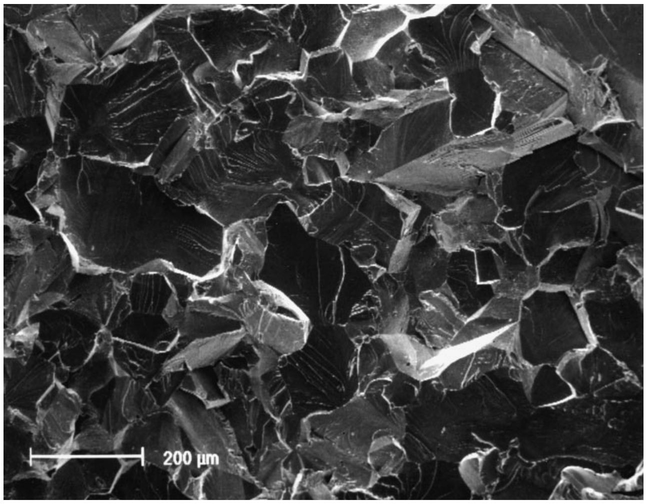

(*a*)

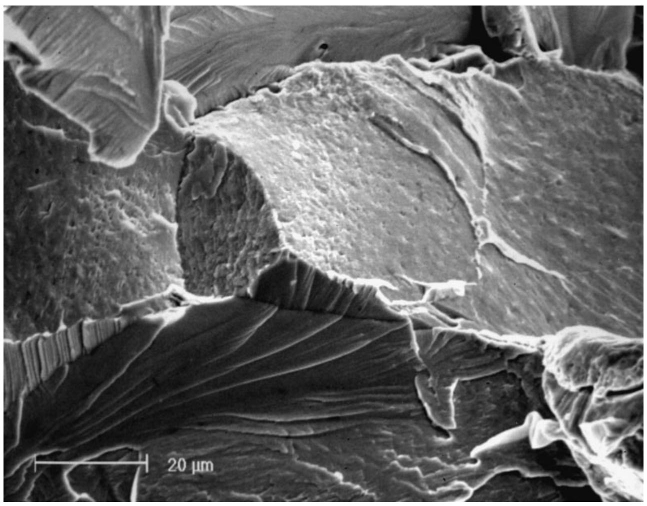

(*b*)

Fig. 16—(*a*) Fracture surfaces of 46Nb-11Cr-34Ti-9Al showing a combination of cleavage and grain boundary facets and (*b*) high-magnification views of grain boundary and cleavage facets.

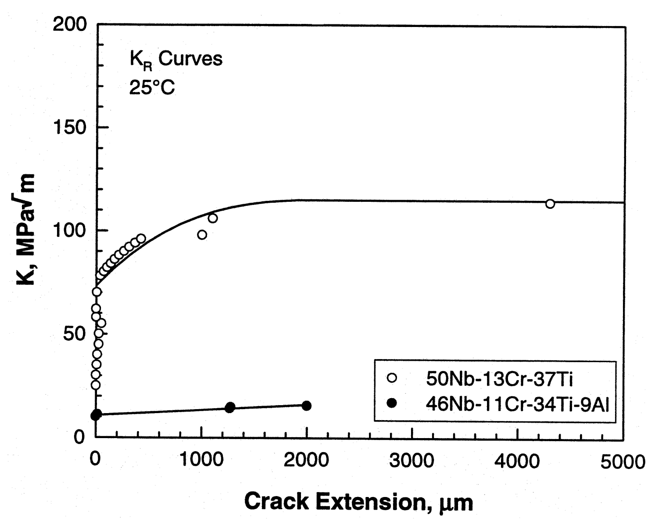

Fig. 17—A comparison of the *K*-resistance curves of Nb-Cr-Ti-Al and Nb-Cr-Ti solid solution alloys.

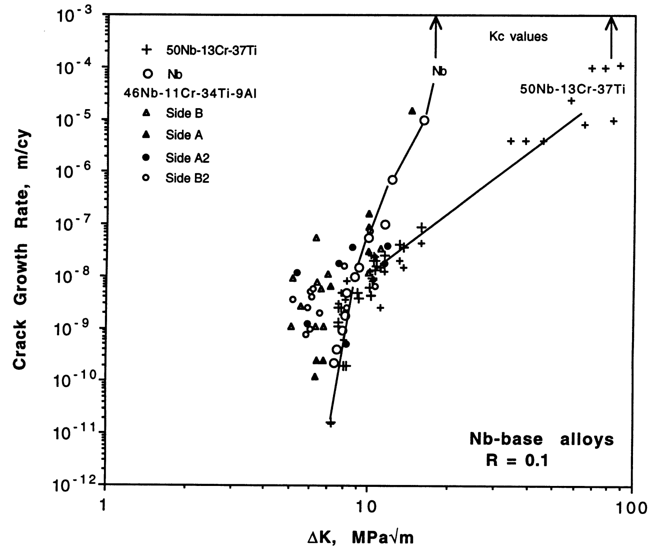

Fig. 18—A comparison of the fatigue crack growth curves of Nb-Cr-Ti-Al and Nb-Cr-Ti solid solution alloys with pure Nb.

procedures described earlier.[16] The results are compared to those for Nb, Nb-13Cr-37Ti, and Nb-10Cr-40Ti-10Al in Table IV. The values of the P–N barrier energy for the LANL-3 alloy are low for both (110) and (112) slip, suggesting that there is a high dislocation mobility on the (110) and (112) planes. On the other hand, the values of the USE are high for both the (110) and (112) slip, implying that the nucleation of dislocations at the crack tip is difficult. The absence of direct observations of slip emission from the crack tip is consistent with the high USE(γ_{us}) values. The ratio of γ_s/γ_{us} is about 1 or less, where γ_s is the surface energy; this value of γ_s/γ_{us} is considerably lower than the value of 3.5 to 6 which is considered necessary for ductile behavior to occur.[20] Because of the high USE value, fracture of the LANL-3 alloy is expected to occur predominantly by cleavage, which is in accordance with experimental observations.

Unlike the Ti addition,[16] an aluminum alloying addition affected the interatomic bonding of the Nb-Cr-Ti-Al alloy in an adverse way. It is unclear whether Al donates electrons to the bonding electrons (d + s) of the alloy or lowers the electron concentration, but, from these results, when compared to previous results,[16] it appears that Al donates d + s electrons to the alloy, thereby increasing bonding between atoms. This effect was anticipated during the design of the alloy, so a substitution was made for Cr, but it appears that Al adds more electrons per atom than does Cr. The effect on mechanical properties of an Al alloying addition is through an increase in the difficulty of nucleating dislocations at the crack tip, a process governed by the USE. The large increase in the USE as a result of the Al alloying addition prevents the emission of dislocations from the crack tip, but promotes the nucleation and propagation of cleavage cracks and, sometimes, grain-boundary cracks. As a consequence, the fatigue and fracture resistance of the Nb-11Cr-34Ti-9Al alloy is lower than that of the Nb-13Cr-37Ti alloy.

Table IV. A Summary of the Composition, Number of d + s Electrons per Atom, Surface Energy (γ_s), Unstable Stacking Energy (γ_{us}), P–N Barrier Energy (U_{P-N}), and Fracture Toughness of LANL-3 and Other Nb-Based Alloys

Alloy	Composition in At. Pct Nb-Cr-Ti-Al	Number of d + s Electrons per Atom	γ_s (J/m^2)	γ_{us} (J/m^2) (110)	γ_{us} (J/m^2) (112)	U_{P-N} (J/m^2) (110)	U_{P-N} (J/m^2) (112)	Plane Strain Fracture Toughness (MPa$\sqrt{m}$)
G	100-0-0-0	5	2.42	0.875	1.52	0.322	0.947	12
D	53-13-37-0	4.76	2.19	0.721	1.26	0.071	0.441	34
F	40-10-40-10	4.66	2.13	0.686	1.18	0.044	0.356	23
LANL-3	46-11-34-9	4.5	2.13	2.02	3.50	0.020	0.250	15

V. CONCLUSIONS

1. An aluminum alloying addition in the amount of 9 to 10 at. pct has an adverse effect on the fatigue and fracture resistance of Nb-Cr-Ti-Al alloys.
2. An aluminum addition increases the USE, prevents the emission of dislocations from the crack tip, and then promotes the nucleation and propagation of cleavage cracks in the Nb-Cr-Ti-Al alloy. Consequently, the fatigue and fracture resistance is lowered by the Al addition.
3. Heat treating the Nb-Cr-Ti-Al alloy at a temperature in the 900 °C to 1500 °C range results in grain-boundary precipitation and, thus, a low fracture toughness for the heat-treated microstructures.
4. Fatigue and quasi-static crack growth occurred in the Nb-Cr-Ti-Al alloys in an intermittently critical manner *via* the nucleation and propagation of cleavage cracks with little plastic flow.
5. The Nb-Cr-Ti-Al alloy exhibited a limited resistance-curve fracture behavior as the result of the crack-wake ligaments formed between cleavage planes.

ACKNOWLEDGMENTS

This research was sponsored by the Air Force Office of Scientific Research (AFSC) under Contract No. F49620-95-0043, Program Monitor, Dr. Spencer Wu. The United States Government is authorized to reproduce and distribute reprints for governmental purposes notwithstanding any copyright notation hereon. Supply of Nb-Cr-Ti-Al alloys by Dr. Dan J. Thoma, Los Alamos National Laboratory (Los Alamos, NM), is acknowledged. Technical assistance by Mr. Byron Chapa and Mr. Jim Spencer and clerical assistance by Ms. Lori Salas and Ms. Patty Soriano, all of Southwest Research Institute, are appreciated.

REFERENCES

1. K.S. Chan: *Metall. Mater. Trans. A*, 1996, vol. 27A, pp. 2518-31.
2. D.L. Davidson, K.S. Chan, and D.L. Anton: *Metall. Mater. Trans. A*, 1996, vol. 27A, pp. 3007-18.
3. K.S. Chan and D.L. Davidson: *JOM*, 1996, vol. 48 (9), pp. 62-68.
4. R.M. Nekkanti and D.M. Dimiduk: *Mater. Res. Soc. Symp. Proc.*, 1990, vol. 194, pp. 175-82.
5. M.G. Mendiratta and D.M. Dimiduk: *Metall. Trans. A*, 1993, vol. 24A, pp. 501-04.
6. J.D. Rigney, P.M. Singh, and J.J. Lewandowski: *JOM*, 1992, vol. 44(8), pp. 36-41.
7. J. Kajuch, J. Short, and J.J. Lewandowski: *Acta Metall. Mater.*, 1995, vol. 43, pp. 1955-67.
8. J. Dipasquale, D. Gahutu, D. Konitzer, and W. Soboyejo: *Materials Research Society Proceedings*, Materials Research Society, Pittsburgh, PA, 1995, vol. 364, pp. 1347-52.
9. M.R. Jackson and K.D. Jones: in *Refractory Metals: Extraction, Processing and Applications*, K. Nona, C. Kiddell, D.R. Sadoway, and R.G. Bautista, eds., TMS, Warrendale, PA, 1990, pp. 311-19.
10. P.R. Subramanian, M.G. Mendiratta, and D.M. Dimiduk: *JOM*, 1996, vol. 48, pp. 33-38.
11. P.R. Subramanian, M.G. Mendiratta, D.M. Dimiduk, and M.A. Stucke: *Mater. Sci. Eng.*, 1997, vol. A239-240, pp. 1-13.
12. M.R. Jackson, B.P. Bewlay, R.G. Rowe, D.W. Skelly, and H.A. Lipsitt: *JOM*, 1996, vol. 48, pp. 39-44.
13. B.P. Bewlay, M.R. Jackson, and H.A. Lipsitt: *Metall. Mater. Trans. A*, 1996, vol. 27A, pp. 3801-08.
14. D.L. Anton and D.M. Shah: *MRS Symp. Proc.*, 1990, vol. 194, pp. 175-82.
15. D.J. Thoma: Ph.D. Thesis, University of Wisconsin, Madison, WI, 1992, available from University Microfilms, Ann Arbor, MI.
16. K.S. Chan and D.L. Davidson: *Metall. Mater. Trans. A*, 1999, vol. 30A, pp. 925-39.
17. K.C. Chen, D.J. Thoma, P.G. Kotula, F. Chu, C.M. Cady, G.T. Gray, P.S. Dunn, D.R. Korzekwa, C. Mercer, and W. Soboyejo: *3rd Pacific Rim Int. Conf. on Advanced Materials and Processing*, M.A. Imam, R. DeNale, S. Hanada, Z. Zhong, and D.N. Lee, eds., TMS, Warrendale, PA, 1998, pp. 1431-36.
18. A. Nagy, J.B. Campbell, and D.L. Davidson: *Rev. Sci. Instrum.*, 1984, vol. 55, pp. 778-82.
19. E.A. Franke, D.J. Wenzel, and D.L. Davidson: *Rev. Sci. Instrum.*, 1990, vol. 62 (5), pp. 1270-79.
20. J.R. Rice: *J. Mech. Phys. Solids*, 1992, vol. 40, pp. 239-71.
21. R.E. Peierls: *Proc. Phys. Soc.*, 1940, vol. 52, pp. 34-37.
22. F.R.N. Nabarro: *Proc. Phys. Soc.*, 1947, vol. 59, pp. 236-394.
23. J.N. Wang: *Mater. Sci. Eng. A*, 1996, vol. A206, pp. 259-69.
24. J.N. Wang: *Acta Mater.*, 1996, vol. 44, pp. 1541-46.
25. D.L. Davidson: *Metall. Mater. Trans. A*, 1997, vol. 28A, pp. 1297-1314.
26. T.G. Li, P.A. Blenkinsop, M.H. Loretto, and N.A. Walker: *Mater. Sci. Technol.*, 1998, vol. 14, pp. 732-37.
27. R. Grylls, S. Perungulan, H.A. Lipsitt, H.L. Faser, R. Wheeler, and S. Banerjee: Paper presented at *'98 TMS Annual Meeting*, San Antonio, TX, Feb. 15–19, 1998.